

# AILERON FLUTTER CALCULATION FOR A SUPERSONIC FUSELAGE-WING CONFIGURATION

**Guowei YANG<sup>1</sup>, Shigeru OBAYASHI<sup>2</sup> and Jiro NAKAMICHI<sup>3</sup>**

(1. Institute of Fluid Science, Tohoku University, Japan.

Email: yang@reynolds.ifs.tohoku.ac.jp)

(2. Institute of Fluid Science, Tohoku University, Japan.

Email: obayashi@ieee.org)

(3. Structures and Materials Research Center, National Aerospace

Laboratory of Japan. Email: nakamichi@nal.go.jp)

*Keywords: Multiblock grid, Numerical simulation, Aeroelasticity, Aileron buzz*

## Abstract

*A fully implicit multiblock aeroelastic solver, coupled thin-layer Navier-Stokes equations with structural equations of motion, has been developed for the flutter simulation on complex aerodynamic configurations. Navier-Stokes equations are solved with LU-SGS subiteration algorithm and a modified Harten-Lax-van Leer Einfeldt-Wada (HLEW) scheme. Structural equations of motion are discretized by a direct second-order differential method with subiteration in generalized coordinates. The transfinite interpolation (TFI) is used for the grid deformation of the blocks neighboring the flexible surface. For the purpose of validation, the boundaries of the flutter speed and frequency of the AGARD 445.6 standard aeroelastic wing are first calculated. Then, the method is used for the prediction of the flutter boundaries of the NAL supersonic transport (SST) fuselage-wing configuration. Finally, for the same model, the aeroelastic instability referred to as aileron buzz is investigated.*

## 1. Introduction

National Aerospace Laboratory (NAL) of Japan has established a research program for scaled experimental supersonic airplanes for five years. A non-powered experimental airplane will be launched in 2002 by a solid rocket booster [1]. Because thin wing-sections and

control surfaces are necessarily used for the high-speed aircraft from the viewpoint of aerodynamic performance, it is important to predict accurately the transonic nonlinear aeroelastic phenomena such as flutter, buffet, and aileron buzz for the structural design of aircraft.

In the last decade, transonic nonlinear aeroelastic analyses have been extensively studied by solving Euler/Navier-Stokes equations coupled with the structural equations of motion [2-5]. However, in these methods, the flow governing equations are only loosely coupled with structural equations of motion, namely, after the aerodynamic loads are determined by solving the flow governing equations, the structural model is used to update the position of body. The coupling contains the error of one time step, thus these methods are always only first-order accuracy in time regardless of the temporal accuracy of the individual solvers of the flow and structural equations.

Tightly coupled aeroelastic approach was first put forward by Alonso and Jameson [6] for 2-D Euler aeroelastic simulation, called dual-time implicit-explicit method. In each real time step, the time-accurate solution is solved by explicit Runge-Kutta time-marching method for a steady problem, so all of convergence acceleration techniques such as multigrid,

residual averaging and local time-step can be implemented in the calculation. In general, about 100 pseudo-time steps are needed for the explicit iterations to ensure adequate convergence, thus the method is still very time-consuming, so far as the authors know only 3-D Euler results were reported recently [7]. Based on the same thought, G. S. L. Goura et al. [8] constructed a first-order implicit time-marching scheme as well as only first-order spatial discretisation in implicit side for the solution of a pseudo steady flow. The second-order temporal and spatial accuracy can be maintained as pseudo steady flow convergence. Euler equations were chosen as the aerodynamic governing equations due to the limitation of computational time.

Melville et al [9] proposed a fully implicit aeroelastic solver between the fluids and structures, in which a second-order approximately factorization scheme with subiterations was performed for the flow governing equations, and the structural equations were cast in an iterative form. Because the restricted number of iterations cannot remove sequencing effects and factorization errors completely at every time step and a relatively small time step was used in their calculation. Nevertheless, a fully implicit aeroelastic Navier-Stokes solver with three subiterations has succeeded in the flutter simulation for an aeroelastic wing [10].

In the flutter calculation, due to the deformation of aeroelastic configuration, adaptive dynamic grid needs to be generated at each time step. At present, most of aeroelastic calculations are only done for an isolated wing with single-block grid topology. For the simple flexible geometry, the grid can be completely regenerated with an algebraic method [2] or a simple grid deformation approach [10]. For the complicated aerodynamic configurations, multiblock grids are usually generated for steady flow simulation. However, for aeroelastic application it is impossible to

regenerate multiblock grids at each time step due to the limitation of computational cost. Multiblock grid deformation approaches need to be used. Recently Potsdam and Guruswamy [11] put forward a multiblock moving grid approach, which uses a blending method of a surface spline approximation and nearest surface point movement for block boundaries, and transfinite interpolation (TFI) for the volume grid deformation. Wong et al. [12] also established a multiblock moving mesh algorithm. The spring network approach is utilized only to determine the motion of the corner points of the blocks and the TFI method is applied to the edge, surface and volume grid deformations.

In addition, structural data may be provided with plate model, but the flow calculations are carried out for the full geometry. The interpolation between fluid and structure grids is required. Infinite and finite surface splines [13] [14] developed for the plate aerodynamics and plate structural model are still main interpolation tools, only the aerodynamic grid needs to be projected on the surface of structural grid before interpolation. Goura et al [15] recently suggested an interpolation method of constant volume transformation (CVT) for the data exchange between fluids and structures based on the local grid information.

In the present paper, a fully implicit multiblock Navier-Stokes aeroelastic solver was developed based on the single-block aeroelastic code implemented by the authors [16]. The purpose of the present work is to simulate the flutter boundary and the aeroelastic phenomenon of aileron buzz on the supersonic transport (SST) designed by the national aerospace laboratory (NAL) of Japan. To validate the developed aeroelastic solver, the flutter boundary on the AGARD 445.6 standard aeroelastic wing is first calculated.

## 2. Governing Equations

## 2.1 Aerodynamic Governing Equations

Aerodynamic governing equations are the unsteady, three-dimensional thin-layer Navier-Stokes equations in strong conservation law form, which can be written in curvilinear space  $\xi, \eta, \zeta$  and  $\tau$  in non-dimensional form as

$$\partial_\tau \hat{Q} + \partial_\xi F + \partial_\eta G + \partial_\zeta H = \text{Re}^{-1} \partial_\zeta H_v + S_{GCL} \quad (1)$$

The viscosity coefficient  $\mu$  in  $H_v$  is computed as the sum of laminar and turbulent viscosity coefficients, which are evaluated by the Sutherland's law and Baldwin-Lomax model.

The source term  $S_{GCL}$  in Equation 1 is obtained from the geometric conservation law for moving mesh, which is defined as

$$S_{GCL} = Q \left[ \partial_\tau J^{-1} + (\xi_\tau / J)_\xi + (\eta_\tau / J)_\eta + (\zeta_\tau / J)_\zeta \right] \quad (2)$$

## 2.2 Structural Governing Equations

Second-order linear structural dynamic governing equations after normalized similar to the flow governing equation can be written as

$$[M] \{\ddot{d}\} + [K] \{d\} = \{F\} \quad (3)$$

where  $[M]$ ,  $[K]$  are the non-dimensional mass and stiffness matrices, respectively.  $\{F\}$ ,  $\{d\}$  are the aerodynamic load and displacement vectors, respectively. For specific aerodynamic configuration, the natural mode shapes and frequencies can be calculated by the finite-element analysis or obtained from experimental influence coefficient measurements. In this study, the data of natural mode shapes and frequencies are calculated by finite-element analysis. Only the first  $N$  modes are considered, the structural equations of motion in generalized coordinates can be written as

$$\ddot{q}_i + 2\zeta_i \omega_i \dot{q}_i + \omega_i^2 q_i = [\Phi]_i^T F / M_i \quad (4)$$

where

$$\omega_i^2 = [\Phi]_i^T [K] [\Phi], \quad M_i = [\Phi]_i^T [M] [\Phi] \quad \{d\} = [\Phi] \{q\}$$

The modal damping is readily added on the left hand side of Equation 4, where  $\zeta_i$  is the damping ratio in the  $i$ th mode. The equation can be written as a first-order system by defining  $S = [q, \dot{q}]$ :

$$\dot{S} + \begin{bmatrix} 0 & -1 \\ \omega_i^2 & 2\omega_i \zeta_i \end{bmatrix} S = \begin{bmatrix} 0 \\ [\Phi]_i^T F / M_i \end{bmatrix} \quad (5)$$

## 3. Numerical Method

LU-SGS method of Yoon and Jameson [17], employing a Newton-like subiteration, is used for solving Equation 1. Second-order temporal accuracy is obtained by utilizing three-point backward difference in the subiteration procedure. The numerical algorithm can be deduced as

$$\begin{aligned} & LD^{-1} U \Delta Q \\ &= -\phi^i \{ (1+\phi) Q^p - (1+2\phi) Q^n + \phi Q^{n-1} \\ &\quad - J \Delta \tau Q^p [ (\xi_\tau / J)_\xi + (\eta_\tau / J)_\eta + (\zeta_\tau / J)_\zeta ]^p \\ &\quad + J \Delta \tau (\delta_\xi F^p + \delta_\eta G^p + \delta_\zeta (H^p - H_v^p)) \} \end{aligned} \quad (6)$$

where

$$L = \bar{\rho} I + \phi^i J \Delta \tau (A_{i-1,j,k}^+ + B_{i,j-1,k}^+ + C_{i,j,k-1}^+)$$

$$D = \bar{\rho} I$$

$$U = \bar{\rho} I - \phi^i J \Delta \tau (A_{i+1,j,k}^- + B_{i,j+1,k}^- + C_{i,j,k+1}^-)$$

and

$$\bar{\rho} = 1 + \phi^i J \Delta \tau (\bar{\rho}(A) + \bar{\rho}(B) + \bar{\rho}(C))$$

$$\phi^i = 1 / (1 + \phi), \quad \Delta Q = Q^{p+1} - Q^p$$

Here,  $\phi = 0.5$ , and  $p$  denotes the subiteration number. The deduced subiteration scheme reverts to the standard LU-SGS scheme for

$\phi = 0$  and  $p = 1$ . In fact, regardless of the temporal accuracy of the left hand of Equation 6, second-order time accuracy is maintained when the subiteration number tends to infinity.

The inviscid terms in Equation 6 are approximated by modified third-order upwind HLLW scheme of Obayashi et al [18]. For the isentropic flow, the scheme results in the standard upwind-biased flux-difference splitting scheme of Roe, and as the jump in entropy becomes large in the flow, the scheme turns into the standard HLLW scheme. Thin-layer viscous term in Equation 6 is discretized by second-order central difference.

The structural equations of motion in generalized coordinates of Equation 5 is discretized by a second order scheme with subiterations of reference [10] as

$$\begin{aligned} & \begin{bmatrix} 1 & -\phi^i \Delta\tau \\ \phi^i \Delta\tau \omega_i^2 & 1 + 2\phi^i \omega_i \zeta_i \Delta\tau \end{bmatrix} \Delta S \\ & = -\phi^i \{ (1 + \phi) S^p - (1 + 2\phi) S^n + \phi S^{n-1} \\ & + \Delta\tau \begin{bmatrix} 0 & -1 \\ \omega_i^2 & 2\omega_i \zeta_i \end{bmatrix} S^p - \Delta\tau \begin{bmatrix} 0 \\ [\Phi]_i^T F^p / M_i \end{bmatrix} \} \end{aligned} \quad (7)$$

where  $\Delta S = S^{p+1} - S^p$

As  $p \rightarrow \infty$ , a full implicit second-order temporal accuracy scheme for aeroelastic computation is formed by the coupling solutions of Equations 6 and 7. For accurate multiblock-grid aeroelastic calculation, the subiteration method is very important not only for eliminating the lagged flowfield induced by lagged multiblock boundary condition but also for removing the sequencing effects between fluids and structures. However, in practical application, only finite subiterations can be used. For example, an approximately factored implicit solver with three subiterations was used in Ref. 10. Similarly, three subiterations are used for the present calculation. Since the restricted number of iterations does not remove sequencing effects and factorization errors at every time step completely, a proper time-step

size needs to be evaluated by numerical tests.

#### 4. Multiblock Grid Deformation

An H-type multiblock grid with 30 blocks depicted in Fig. 1 is used for the aeroelastic calculations of the SST wing/fuselage model. The surface grid is distributed as shown in Fig. 2, which contains 4 zones, 3 zones for fuselage and 1 zone for the wing. Total 8 zones are distributed on the whole surface of SST. Aileron surface is distributed at  $12 \times 13$  grid points in the span- and chord-wise directions, respectively.

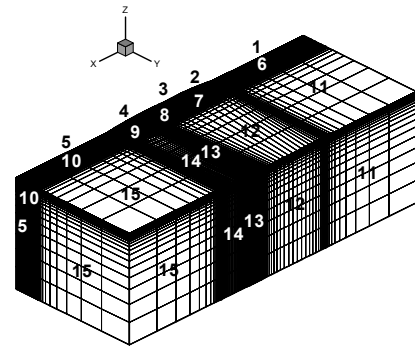


Fig. 1 Multiblock grid with 30 blocks for SST

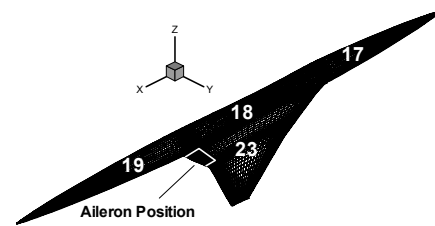


Fig. 2 Surface grid distribution on SST

In the present aeroelastic calculations, only the structural deformation of wing is considered, the blocks containing the fuselage surface and the blocks away from the flexible wing can be fixed. The grid deformations only need to be performed for the 12 blocks adjacent to the deforming wing. The computational cost

for the grid deformation can be decreased largely.

The TFI method [12] is applied to deform the grid blocks. Based on the known deformations of the flexible body and the parameterized arc-length values of the original grid, 1-D, 2-D and 3-D TFI methods can be used to interpolate deformation values in inner grid points. Then the deformations are added to the original grid to obtain the new multiblock grid. For the small and moderate aeroelastic deformation, the present method maintains the grid quality of the original grid and maximizes the re-usability of the original grid. For the aileron deflection, a simple sheared mesh is used and a gap is introduced between the ends of the aileron and wing to allow sufficient space for the moving sheared mesh. The present solver assumes the aileron oscillation of small amplitude. For aileron flutter analyses, the tendency of flow stability can be analyzed from the dynamic response of aileron at relatively small magnitude.

### 5. Data Transformation

In the present aeroelastic calculations, the structural modal data are provided with the plate model and only normal deformation is considered. However, the real geometry is used for the fluid solution. Then the problem of passing information between the fluid and structural grids becomes very complicated. In the paper, the fluid grid is first projected to the surface of structural grid. The deformations on the projected fluid grid points are interpolated by the infinite plate spline (IPS) [13]. The new geometry can then be obtained by adding the deformations in the normal direction to the old one.

IPS is to obtain an analytic function  $w(x, y)$ , which passes through the given structural deflections of  $N$  points  $w_i = w(x_i, y_i)$ . The

static equilibrium equation of  $D\nabla^4 w = q$  should be satisfied, where  $D$  is the plate elastic coefficient,  $q$  is the distributed load on the plate. The solution by superposition of fundamental functions can be written as

$$w(x, y) = a_0 + a_1x + a_2y + \sum_{i=1}^N F_i r_i^2 \ln r_i^2 \quad (8)$$

$$\text{where } r_i^2 = (x - x_i)^2 + (y - y_i)^2$$

The  $N + 3$  coefficients  $(a_0, a_1, a_3, F_1, F_2, \dots, F_N)$  in Equations (8) can be solved through the function passes the given structural deflections of  $N$  and three additional conditions of the conservation of total force and moment:

$$\sum_{i=1}^N F_i = 0, \quad \sum_{i=1}^N x_i F_i = 0 \quad \text{and} \quad \sum_{i=1}^N y_i F_i = 0 \quad (9)$$

Then the deformations of aerodynamic grid points can be evaluated with the function (8). The above linear displacement transformation can be written in the form  $\delta S_a = [G]\delta S_s$ , where

$\delta S_a$  and  $\delta S_s$  are the displacement vectors defined on the aerodynamic grid and the structural grid, respectively

The force transformation from the fluid to structural grids can be calculated with the principle of virtual work of  $F_s = [G]^T F_a$ , where

$F_s$  and  $F_a$  represent the forces on the structural and fluid grids, respectively. The principle of virtual work can guarantee the conservation of energy between the fluid and structural systems.

In the practical application, the LU decompositions of the coefficients matrix and its transpose matrix of the equation groups of (8) and (9),  $a_0, a_1, a_3, F_1, \dots, F_N$  as unknown



quantities, are pre-calculated and stored in the code. For the flutter simulation of aileron oscillation on SST, interpolations are applied on the aileron and wing separately since deformation is discontinuous between the zones of the aileron and wing.

## 6. Results and Discussions

### 6.1 AGRAD 445.6 Wing

Aeroelastic wind-tunnel experiment is intrinsically destructive and hence much more expensive than a similar rigid-body experiment. Therefore, it is hard to find a suitable experimental data to validate the developed aeroelastic solver. The unique complete aeroelastic experiment is available for the AGARD 445.6 standard aeroelastic wing [19], which has been used to validate flutter simulations in most of publications. The disadvantage of the test is that the nonlinear character is relatively weak due to a thin wing, and thus linear, Euler and Navier-Stokes equations all can predict good results comparing with experimental data. However, in the absence of a better experiment, the experiment is still used to evaluate the current method.

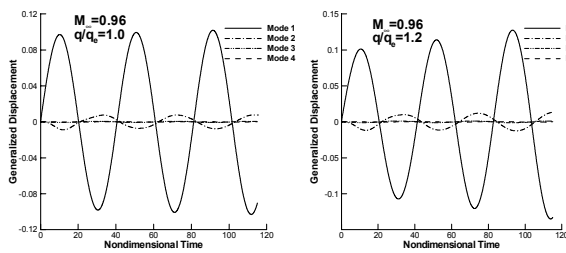


**Fig. 3 Dynamic response of first four modes:**

$M_\infty = 0.96$  and  $q/q_e = 1.0, 1.2$

The AGARD 445.6 wing model [19] was constructed of laminated mahogany and was essentially homogeneous. The wing has an aspect ratio 1.6525, a taper ratio of 0.6576, a quarter-chord swept angle of 45 deg and a

NACA 65A004 airfoil section. Instead of a single-block grid, a H-type multiblock grid is used for the flutter simulations. The number of total grid cells is 420,000.

The first four structural modes and natural frequencies provided in the reference [19] are used for the present computations and a nondimensional time step is taken as  $\Delta t = 0.05$ . All simulations are started from its corresponding steady flow. Each Mach number is run for several dynamic pressures to determine the flutter point. As the dynamic pressure is varied, the freestream density and Mach number are held fixed and Reynolds number is allowed to vary. At  $t = 0$ , a small initial velocity perturbation of 0.0001 for the first bending mode is applied to the wing.

The responses of the first four modes are shown in Figure 3 for the  $M_\infty = 0.96$  case at dynamic pressures  $q/q_e = 1.0$  and 1.2, where the experimental flutter dynamic pressure is  $q_e = 61.3 \text{ lbf/ft}^2$ . The dominant mode appears to be the first bending mode, and only second mode has some effects to the first mode. The amplification factor of the first bending mode is analyzed, which is defined as the ratio of the magnitude of a peak with the magnitude of the previous peak of the same sign. Its corresponding response frequency is determined from the period between these two peaks. For the two cases, the amplifications and response frequencies are  $AF = 1.023$ ,  $\omega = 84.135 \text{ rad/sec}$  for  $q/q_e = 1.0$ , and  $AF = 1.093$ ,  $\omega = 89.559 \text{ rad/sec}$  for  $q/q_e = 1.2$ . Then the dynamic pressure and frequency for flutter ( $AF = 1.0$ ) can be interpolated linearly as  $q/q_e = 0.934$ ,  $\omega = 82.353 \text{ rad/sec}$ .

With the method, the flutter boundary and

frequency over the Mach number range of 0.338 to 1.141 are calculated and compared with experimental data in Fig. 4. The typical transonic dip phenomenon is well captured. In the subsonic and transonic range, the calculated flutter speeds and frequencies agree well with experimental data, however, in the supersonic range, the present calculation overpredicts the experimental flutter points similar to other computations.

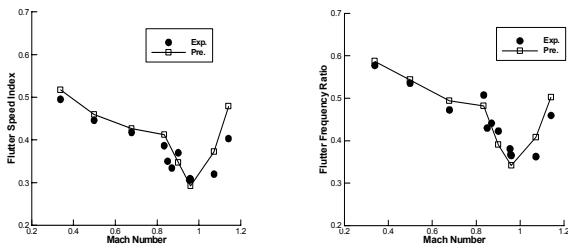


**Fig. 4 Flutter speed and frequency for the AGARD 445.6 wing**

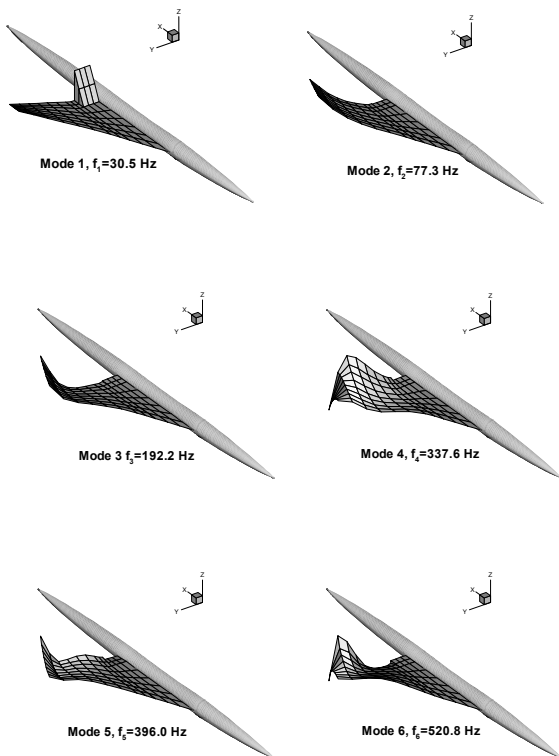


**Fig. 5 First six modes and natural frequencies for the SST aileron-weakened structural model**

**6.2 SST Wing/Fuselage Model**

Aeroelastic flutter simulations on the SST wing/fuselage configuration are performed for two weakened structural models. One is the wing-weakened structural model for the prediction of the wing flutter boundary. First eleven structural modes are considered in the calculation, in which the lowest mode frequency is the first bending mode. The frequencies of first four modes are 18.37 Hz, 51.14Hz, 86.96Hz and 122.60 Hz. Another is the aileron-weakened structural model for the investigation of aileron buzz. For the experiment of aileron buzz, the fuselage and main wing are rigid, however, the aileron is attached to the main wing by a spring with different strength to simulate the hinge stiffness. Figure 5 shows the first six structural modes and natural frequencies of the weakened structural model. For the model, the oscillating mode of aileron has the lowest natural frequency of 30.5 Hz. Experiments wish the nonlinear aeroelastic phenomenon of aileron buzz appears on the weakened structural model at some Mach numbers.

The multiblock and surface grids are shown in Figures 1 and 2 before. The number of total grid points for the following calculations is 834,960. A small modal damping coefficient  $\zeta_i = 0.02$  was added in the structural equations of motion. The time-step size is taken as 0.01.

**6.2.1 Flutter Boundary**

The flutter boundary of the SST wing-weakened structural model can be determined with the same method as the standard aeroelastic wing. Figure 6 shows the dynamic responses of the first six modes at  $M_\infty = 0.90$  and the total pressure  $P_0 = 40Kpa$  and  $50Kpa$ , respectively. The flutter point is determined by the dominant blending mode. Due to highly nonlinearity of flow, in some cases, determining the flutter point may be

ambiguous. Figure 7 gives the closely neutral dynamic responses at  $M_\infty = 0.95$  and  $0.98$ . The flutter boundary and frequency for the wing-weakened structural model are depicted in Fig. 8. The typical transonic dip phenomenon is also captured.

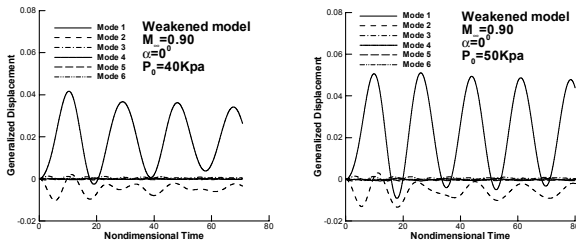


**Fig. 6 Dynamic responses of first six modes at  $M_\infty = 0.90$  and  $P_0 = 40\text{Kpa}, 50\text{Kpa}$**

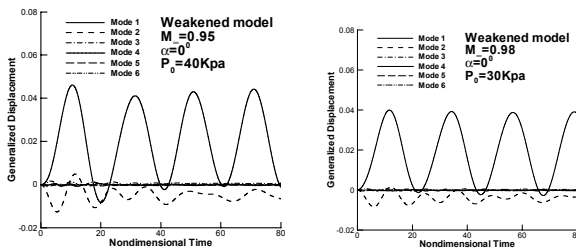


**Fig. 7 Dynamic responses of first six modes at  $M_\infty = 0.95$  and  $0.98$**

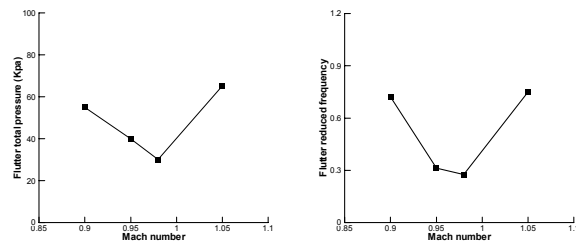


**Fig. 8 Flutter total pressure and reduced frequency for the wing-weakened structural model**

**6.2.2 Aileron Buzz**

Aileron flutter calculations are implemented for three transonic Mach numbers of 0.95, 0.98 and 1.05 under the fixed total pressure of 85 Kpa and angle of attack of 0 degree. Figure 9 shows dynamic responses of first sixth modes

and aileron oscillation angle. For the aileron weakened structural model, the dominant mode is the aileron oscillation mode, which is stable at Mach number of 0.95 and diverges at Mach numbers of 0.98 and 1.05. The divergence speed at Mach number of 0.98 is faster than that of Mach number of 1.05. The change of aileron oscillation angle has the same tendency as dynamic response of the first mode. At Mach number of 0.98, the amplitude of the aileron oscillation angle becomes larger and larger until the calculation breaks down due to the use of a simple sheared grid deformation for the aileron deflection.

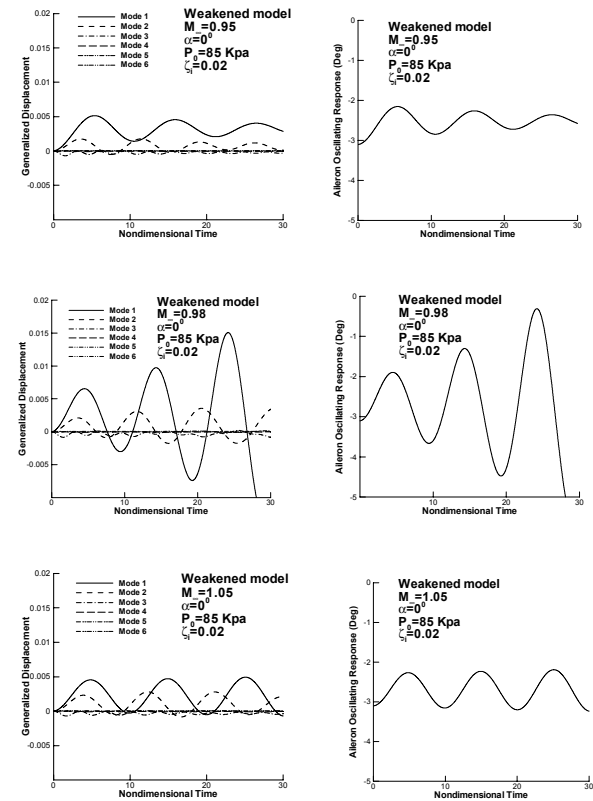


**Fig. 9 Dynamic responses of first six modes and aileron oscillation angle for the SST aileron-weakened structural model**

The pressure contours at Mach number of 0.98 are shown in Figure 10, which corresponds two typical positions of aileron oscillation. On the upper surface of the wing, the shock wave becomes weaker as the aileron oscillates upward and becomes stronger as the



aileron deflects downward, and the flow behaves just contrary on the lower surface of the wing. Corresponding to general theoretical analysis, the flow instability referred to as aileron buzz is induced by a stronger shock alternately moving on the upper and lower surfaces of wing.

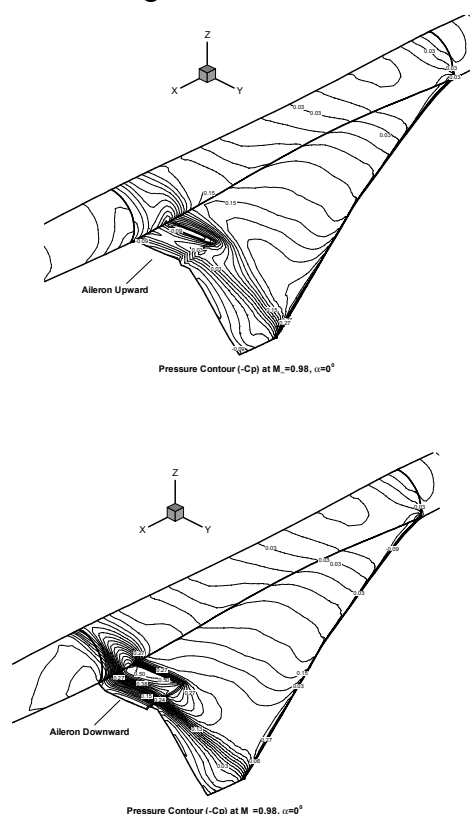


**Fig. 10 Pressure contours of aileron oscillation for the aileron-weakened structural model at  $M_\infty = 0.98$**

## 7. Concluding Remarks

A fully implicit aeroelastic solver has been developed for flutter simulation on complex configuration through the tightly coupled solution of Navier-Stokes equations and structural equations of motion. The flutter boundary of AGARD 445.6 standard aeroelastic wing was first calculated and compared with the experimental results to validate the solver. Then the method was used for the prediction of the flutter boundary and

the aeroelastic instability referred to as aileron buzz on two SST weakened structural wing/fuselage models. The typical transonic dip phenomenon was captured. Aileron buzz has been simulated at the Mach numbers of 0.98 and 1.05, which is induced by the movement of the shock wave alternately on the upper and lower surfaces.

## References

- [1] K. Sakata: Supersonic Experimental Airplane Program in NAL and its CFD-Design Research Demand, *2<sup>nd</sup> SST-CFD Workshop*, pp. 53-56, 2000.
- [2] G. P. Guruswamy: Vortical Flow Computations on Swept Flexible Wings Using Navier-Stokes Equations, *AIAA Journal*, Vol. 28, pp. 2077-2084, 1990.
- [3] E. M. Lee-Rausch and J. T. Batina: Wing Flutter Computations Using an Aeroelastic Model Based on the Navier-Stokes, *Journal of Aircraft*, Vol. 33, pp. 1139-1147, 1996.
- [4] S. A. Goodwin, R. A. Weed, L. N. Sankar and P. Raj: Towards Cost-Effective Aeroelastic Analysis on Advanced Parallel Computing Systems, *Journal of Aircraft*, Vol. 36, No. 4, pp. 710-715, 1999.
- [5] P. M. Hartwich, S. K. Dobbs, A. E. Arslan and S. C. Kan, Navier-Stokes Computations of limit-Cycle Oscillations for a B-1-Like Configuration, *Journal of Aircraft*, Vol. 38, No. 2, pp. 239-247, 2001.
- [6] J. J. Alonso and A. Jameson: Fully-Implicit Time-Marching Aeroelastic Solutions, *AIAA Paper 94-0056*. 1994.
- [7] F. Liu, J. Cai, Y. Zhu, H. M. Tsai and A. S. F. Wong: Calculation of Wing Flutter by a Coupled Fluid-Structure Method, *Journal of Aircraft*, Vol. 38, No. 2, pp. 334-242, 2001.
- [8] G. S. L. Goua, K. J. Badcock, M. A. Woodgate and B. E. Richards: Implicit Method for the Time Marching Analysis of Flutter, *The Aeronautical Journal*, Vol. 105,

- pp.199-214, 2001.
- [9] R. B. Melville, S. A. Morton and D. P. Rizzetta: Implementation of a Fully-Implicit, Aeroelastic Navier-Stokes Solver, *AIAA paper 97-2039*, 1997.
- [10] R. E. Gordiner and R. B. Melville: Transonic Flutter Simulations Using an Implicit Aeroelastic Solver, *Journal of Aircraft*, Vol.37, pp.872-879, 2000.
- [11] M. A. Potsdam and G. P. Guruswamy: A Parallel Multiblock Mesh Movement Scheme for Complex Aeroelastic Applications, *AIAA Paper 01-0716*. 2001.
- [12] A. S. F. Wong, H. M. Tsai, J. Cai, Y. Zhu and F. Liu: Unsteady Flow Calculations with a Multi-Block Moving Mesh Algorithm, *AIAA Paper 00-1002*. 2000.
- [13] R. L. Harder and R. N. Desmarais: Interpolation Using Surface Splines, *Journal of Aircraft*, Vol. 9, pp.189-191, 1972.
- [14] K. Appa: Finite-Surface Spline, *Journal of Aircraft*, Vol. 26, pp.495-496, 1989.
- [15] G. S. L. Goura, K. J. Badcock, M. A. Woodgate and B. E. Richards: A Data Exchange Method for Fluid-Structure Interaction Problems, *The Aeronautical Journal*, Vol. 105, pp.215-221, 2001.
- [16] G. W. Yang and S. Obayashi: Transonic Aeroelastic Calculation with Full Implicit Subiteration and Deforming Grid Approach, *Aeronautical Numerical Simulation Technology Symposium 2001*, Tokyo, June, 2001.
- [17] S. Yoon and A. Jameson: Lower-Upper Symmetric –Gauss-Seidel Method for the Euler and Navier-Stokes Equations, *AIAA Journal*, Vol. 26, pp. 1025-1026, 1988.
- [18] S. Obayashi and G. P. Guruswamy: Convergence Acceleration of a Navier-Stokes Solver for Efficient Static Aeroelastic Computations, *AIAA Journal*, Vol.33, pp.1134-1141, 1995.
- [19] E. C. Jr. Yates: AGARD Standard Aeroelastic Configurations for Dynamic Response I-Wing 445.6, *AGARD-R-765*, 1988.